frontiers | Frontiers in Environmental Science

METHODS
published: 08 June 2022
doi: 10.3389/fenvs.2022.890343

A Novel Branch and Bound Pure Integer Programming Phase Unwrapping Algorithm for Dual-Baseline InSAR

Hui Liu[1,2,3]*, *JiaWei Yue*[4], *QiHuan Huang*[4]*, *GeShuang Li*[5] and *Min Liu*[3]

[1]Collaborative Innovation Center of Geo-Information Technology for Smart Central Plains, Zhengzhou, China, [2]Key Laboratory of Spatiotemporal Perception and Intelligent Processing, Ministry of Natural Resources, Zhengzhou, China, [3]College of Surveying and Geo-Information, North China University of Water Resources and Electric Power, Zhengzhou, China, [4]School of Earth Sciences and Engineering, Hohai University, Nanjing, China, [5]Zhengzhou Communications Planning Survey and Design Institute, Zhengzhou, China

Phase unwrapping (PU) is an important bottleneck restricting the practical application of the interferometric synthetic aperture radar (InSAR) technique. In view of the similarity between solving the ambiguity number of integral cycles in PU for dual-baseline InSAR and pure integer programming (PIP) problem in science of overall planning, a new branch and bound PIP-PU algorithm for dual-baseline InSAR is proposed. A PIP-PU model with the intercept on the vertical axis as the objective function and a ray as the constraint condition is first constructed. Then, how to solve the ambiguity number is given in detail by graphical means. Finally, the axis symmetry theory is introduced to further improve PU efficiency. The proposed algorithm has the advantages of better unwrapping ability even in phase under-sampling areas and abrupt topographic change areas and lower requirement of the baselines. Through two sets of simulated data and one set of real data experiments, the feasibility, effectiveness, and practicability of this proposed algorithm are verified, respectively. In addition, compared with the branch-cut method, quality-guided method, least square method, and minimum cost flow method, the proposed method has the highest accuracy and suboptimal unwrapping efficiency.

Keywords: interferometric synthetic aperture radar, pure integer programming, phase unwrapping, dual-baseline, slack problem, branch and bound method

OPEN ACCESS

Edited by:
Lei Zhang,
Tongji University, China

Reviewed by:
Yandong Gao,
China University of Mining and Technology, China
Hanwen Yu,
University of Electronic Science and Technology of China, China

***Correspondence:**
Hui Liu
lh860801@163.com
QiHuan Huang
InSAR@hhu.edu.cn

Specialty section:
This article was submitted to Environmental Informatics and Remote Sensing, a section of the journal Frontiers in Environmental Science

Received: *05 March 2022*
Accepted: *22 April 2022*
Published: *08 June 2022*

Citation:
Liu H, Yue J, Huang Q, Li G and Liu M (2022) A Novel Branch and Bound Pure Integer Programming Phase Unwrapping Algorithm for Dual-Baseline InSAR. Front. Environ. Sci. 10:890343. doi: 10.3389/fenvs.2022.890343

INTRODUCTION

The interferometric synthetic aperture radar (InSAR), characterized by the advantages of all-time, all-weather, and high-resolution, has been developed as an indispensable weapon for measuring topography and ground deformation. However, phase unwrapping (PU), an irreversible problem, is an important bottleneck restricting the practical application of the InSAR technique (Wang et al., 2002; Liao and Lin,. 2003; Tang et al., 2018; Liu et al., 2019). The traditional single-baseline PU algorithms can be roughly divided into path-following type (Goldstein et al., 1988; Flynn 1997; Zhong et al., 2011), minimum norm type (Takajo and Takahashi, 1988; Long et al., 2008; Chen et al., 2012), and optimal estimation type (Costalltilli, 1988; Liu et al., 2011; Liu et al., 2017; Xie et al., 2020) according to different strategies. The path-following algorithms are difficult to set a suitable integration path and even form an isolated area

that the integration path cannot reach when there are many phase residual points in the interferogram, thereby resulting in a decrease in unwrapping accuracy or even failure. There is no global error in the minimum norm algorithms, but they may have a local error in the unwrapping result at any point (Jin et al., 2014). However, the single-baseline algorithms are based on the assumption of phase continuity, the real terrain undulations usually cannot meet the requirement of terrain continuity. Therefore, the predecessors later proposed the multibaseline PU technique (Yu and Lan,. 2016; Yu et al., 2020; Yu and Hu. 2021), which can overcome the limitations of terrain factors by adding multiple interferometric phases and reduce the influence of phase under-sampling and spectrum aliasing, thereby improving the accuracy and reliability of PU. The multibaseline PU algorithms mainly include the Chinese remainder theorem method (Wei et al., 1994; Zhang et al., 2011a; Jiang et al., 2019), the difference filtering method (Zhang et al., 2011b; Jin et al., 2012; Liu and Xu. 2018), the maximum likelihood method (Si et al., 2017; Dong et al., 2018; Ma et al., 2020), the cluster-analysis method (Yu et al., 2011; Liu. 2015; Jiang et al., 2017), and the minimum norm method (Ge et al., 2013; Yu and Bao. 2013; Liu H et al., 2015; Gao et al., 2019). The Chinese remainder theorem method regards PU as the problem of solving congruence equations and uses the extended Euclidean algorithm to solve the ambiguity numbers. The difference filtering method introduces the idea of difference filtering into the multibaseline PU and guides the unwrapping for long-baseline interferogram through the unwrapping result of the short-baseline interferogram, which solves the problem of phase under-sampling of long-baseline interferogram. The maximum likelihood method uses multiple complex SAR images and maximum likelihood estimation criteria to obtain the long-baseline unwrapping phase. The cluster-analysis method first clusters all pixel into different groups and then unwraps phases of pixels group by group using the information of the cluster center. The minimum norm method uses the phase gradient of each baseline interferogram and the idea of difference to improve the accuracy of long-baseline unwrapping. In recent years, Yu et al. (2019) and Zhou et al. (2021) proposed to use artificial intelligence methods to solve the phase unwrapping problem for single-baseline or multibaseline.

However, whether it is a single-baseline or multi-baseline algorithm, the essence of PU is to solve the number of integral cycles between interferometric phases in one entire interferogram (Jin et al., 2014), to restore the interferometric phase information from interval $[-\pi, \pi)$ to interval $[-m\pi, m\pi)$. Pure integer programming (PIP) is a discrete optimization problem in which all decision variables are integers. From the point of seeking integer solutions, both have similarities in common. Integer programming (IP) was formed in 1958 as an independent branch. It mainly solves the derivative problems of the original problem step by step and determines the destination of the source problem through the solution of the slack problem, until there are no more unsolved derivative problems (Levitin and Tichatschke.1998). This theory has been widely used in the fields of transportation and computer communication (Ikram et al., 2020; Omer et al., 2020), but it is rarely studied in the InSAR field. The term IP was mentioned in Liu H T et al. (2015); in fact, this theory is not used to solve the problem, but the minimum norm method is used. Open source software SYMPHONY was used to solve the integer linear programming (ILP) problem related to PU in Markus, (2016); but in fact, it is built on the basis of the minimum cost flow (MCF) method, and it just generalized the MCF method. Two-stage programming approach (TSPA) algorithm uses a single-baseline ambiguity number integer programming model in the second step, but it actually uses the L1 norm idea to unwrap the phase (Yu and Lan,. 2016). A mixed-integer programming model is constructed by setting the inclined plane equation based on the idea of sharing an ambiguity number in a local area in Jin et al. (2018). However, this local area assumption itself limits the practicability of the algorithm, and it is impossible to obtain the ideal unwrapping effect in difficult unwrapping areas such as phase under-sampling. At present, there is still no literature on solving the PU problem using PIP algorithm. In this article, the PU problem is transformed into a PIP problem. The PIP–PU model is constructed, the axis symmetry theory is introduced, and a new branch and bound PIP–PU algorithm is proposed based on the basic principles of dual-baseline InSAR.

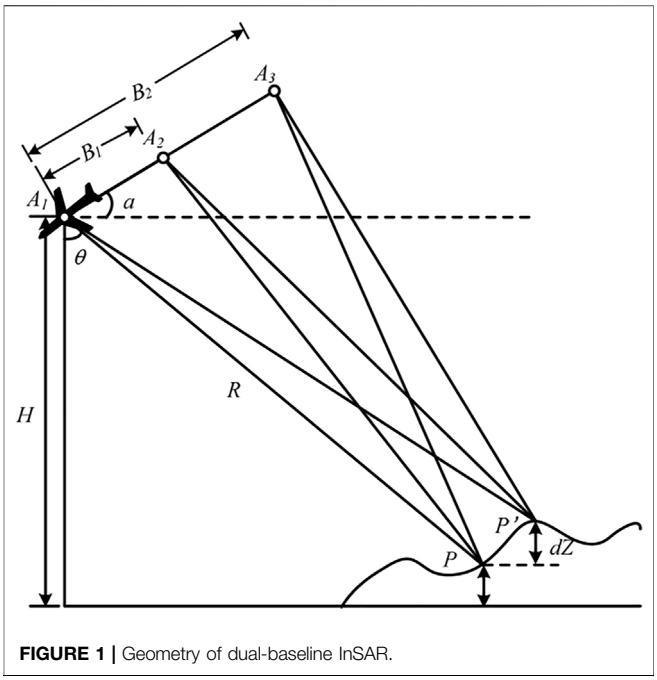

FIGURE 1 | Geometry of dual-baseline InSAR.

The remainder of this article is organized as follows: **Section 2** proposes the new idea of constructing the PIP–PU model. **Section 3** describes the branch and bound PIP–PU algorithm. **Section 4** shows the performances of the proposed method using three sets of examples from simulated data to real data and compares with four mainstream algorithms of commercial software including the branch-cut method, quality-guided method, least squares (LS) method, and MCF method. Finally, a concise conclusion is drawn in **Section 5**.

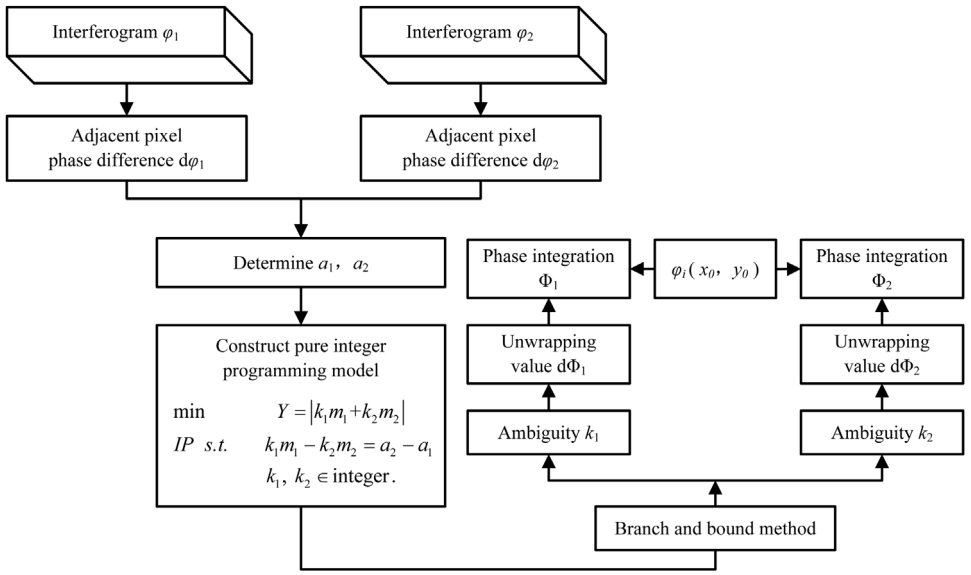

FIGURE 2 | Branch and bound PIP–PU process for dual-baseline InSAR.

THE PRINCIPLE OF PURE INTEGER PROGRAMMING PHASE UNWRAPPING

The geometry of dual-baseline InSAR is shown in **Figure 1**. Assuming that the antenna phase centers A_1, A_2, and A_3 are on the same straight line, two baselines B_1 and B_2 can be formed. The horizontal angle of the baseline is α. The incidence angle and slant distance of the interested point P are θ and R, respectively.

Assuming that the wrapped phases corresponding to the dual-baseline InSAR are φ_1 and φ_2, respectively, the same relative elevation dZ and each interferometric phase differential $d\varphi_i\,(i = 1, 2)$ have the following relationship (Zhang et al., 2011a):

$$dZ = \frac{1}{2\pi} \cdot \frac{\lambda R \sin\theta}{B\cos(\theta - \alpha)} \left(d\varphi_{\mathrm{i}} + 2k_i\pi\right), \tag{1}$$

where λ is the radar wavelength and k_i is the ambiguity number of $d\varphi_i$. Let $B_0 = [B_1, B_2]$ be the least common multiple of the two baselines B_1 and B_2, and $m_i = B_0/B_i\,(i = 1, 2)$ be the modulus, we can obtain the following:

$$\frac{2\pi B_0 \cos(\theta - \alpha)}{R\lambda \sin\theta} \cdot dZ = d\varphi_{\mathrm{i}} \cdot m_i + 2\pi k_i m_i. \tag{2}$$

If $X = \frac{B_0\cos(\theta-\alpha)}{R\lambda\sin\theta} \cdot dZ$, $a_i = \frac{d\varphi_i \cdot m_i}{2\pi}$, the equations of the ambiguity numbers k_1 and k_2 of the wrapped phase differential for dual-baseline InSAR can be established:

$$\begin{cases} X = a_1 + k_1m_1, \\ X = a_2 + k_2m_2, \end{cases} \tag{3}$$

where a_1 and a_2 are the wrapped phase differential functions of interferograms, m_1 and m_2 are the modulus, and X can be regarded as an unknown parameter.

In view of the similarity between solving the ambiguity number of 2π integral cycles and PIP problem, the dual-baseline InSAR PU problem can be transformed into a PIP problem. **Figure 2** shows the branch and bound PIP–PU process for dual-baseline InSAR.

Adding the two equations in **Eq. 3**:

$$2X = a_1 + a_2 + k_1m_1 + k_2m_2. \tag{4}$$

There are infinitely many solutions for the two equations corresponding to three unknown parameters. For the phase ambiguity number that needs to be solved, it is a set of minimum integer solutions that satisfy the equation system, which just corresponds to the fundamental solution system in the general solution of a homogeneous system of equations in linear algebra (Department of Mathematics of Tongji University. 2003). That is, the absolute value of the corresponding X is the smallest. After the phase difference dφ_{i} and the modulus m_i being determined, a_1 and a_2 can be calculated. Therefore, solving the minimum value of X is equivalent to finding the minimum value of **Eq. 5**:

$$Y = |k_1m_1 + k_2m_2|. \tag{5}$$

Eqs 3–5 can be transformed into the IP model as follows:

$$\begin{aligned} &\min && Y = |k_1m_1 + k_2m_2|, \\ &IP\ s.t. && k_1m_1 - k_2m_2 = a_2 - a_1, \\ & && k_1, k_2 \in \text{integer}. \end{aligned} \tag{6}$$

A NEW BRANCH AND BOUND PIP–PU ALGORITHM

To solve the integer programming problem, it is necessary to first remove the integer constraints and convert it into a linear programming (LP) model to solve the slack problem (**Eq. 7**). The solution process of the branch and bound PIP–PU algorithm for dual-baseline InSAR is shown in **Figure 3**:

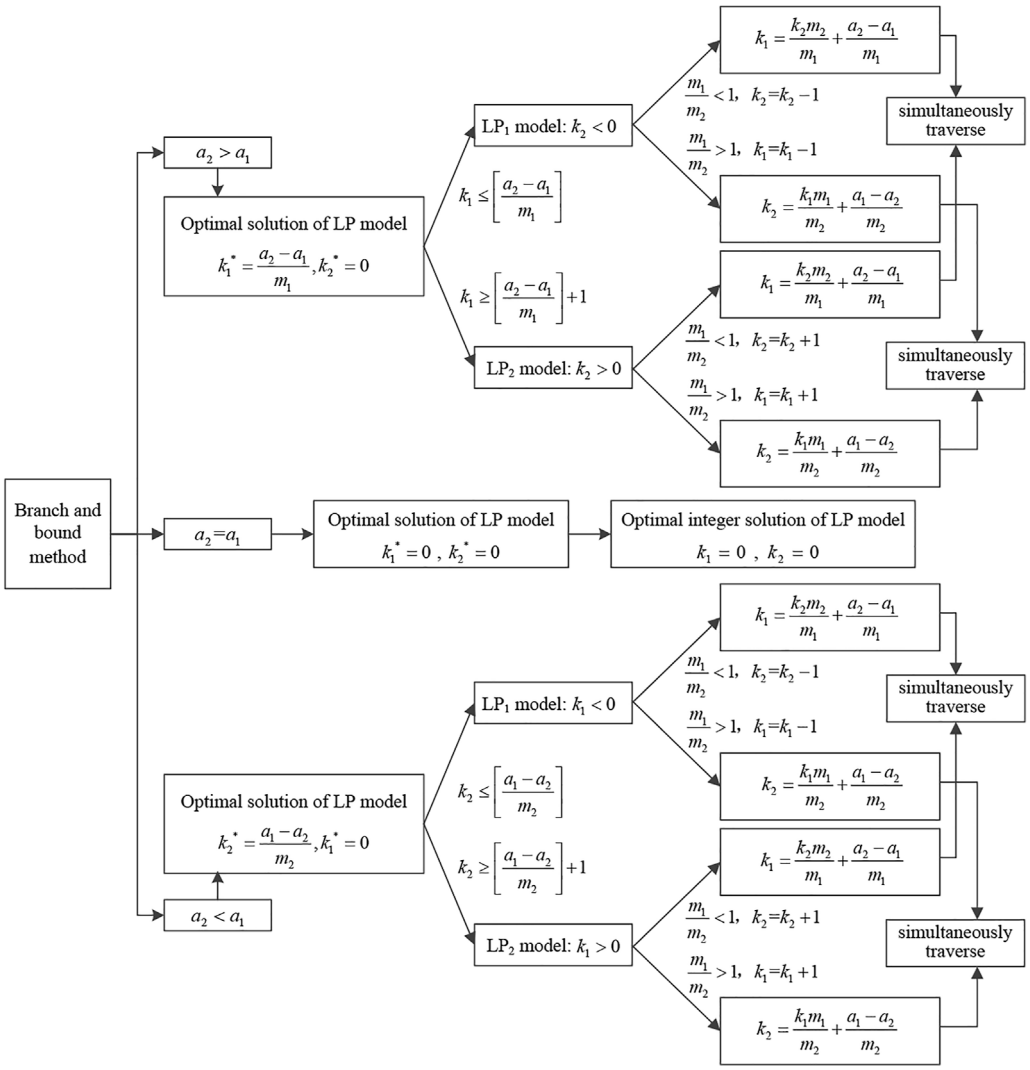

FIGURE 3 | Solution process of branch and bound PIP–PU algorithm for dual-baseline InSAR.

$$\begin{aligned} &\min \quad Y = |k_1 m_1 + k_2 m_2|, \\ &LP\ s.t. \quad k_1 m_1 - k_2 m_2 = a_2 - a_1. \end{aligned} \tag{7}$$

As can be seen from **Figure 3**, the basic idea of the branch and bound PIP–PU algorithm is as follows: using the relationship of a_i as the judgment condition, first ensure that the optimal solution falls on the positive axis of the Cartesian coordinate system, and set it as the critical point. Then, take one of the ambiguity numbers as an integer variable, add a step size every time to both sides of the coordinate axis to traverse, and use the constraint condition as an equation to solve the value of the number to verify whether the integer condition holds, until the two ambiguity numbers are both integer which stops traversing. Since the principle of simultaneous traversal of ambiguity numbers on both sides of the coordinate axis is the same, for simplicity of discussion, the following part only shows the case in which the traversal of the ambiguity number to positive direction of the coordinate axis and traversal in the negative direction can solve the ambiguity number in the same way.

Ambiguity Number Solving Method

The solution of the ambiguity number can be divided into basic model and auxiliary model according to the relationship of between a_1 and a_2 . **Figure 4A** shows the basic model with positive intercept of constraint condition and horizontal axis when $a_2 > a_1$. **Figure 4B** shows the auxiliary model with positive intercept of constraint condition and vertical axis when $a_2 < a_1$.

The equation that k_1 as the independent variable and k_2 as the dependent variable can be set up, and the constraint condition is:

$$k_2 = \frac{k_1 m_1}{m_2} + \frac{a_1 - a_2}{m_2}. \tag{8}$$

The optimal solution of the basic and auxiliary models can be solved, respectively:

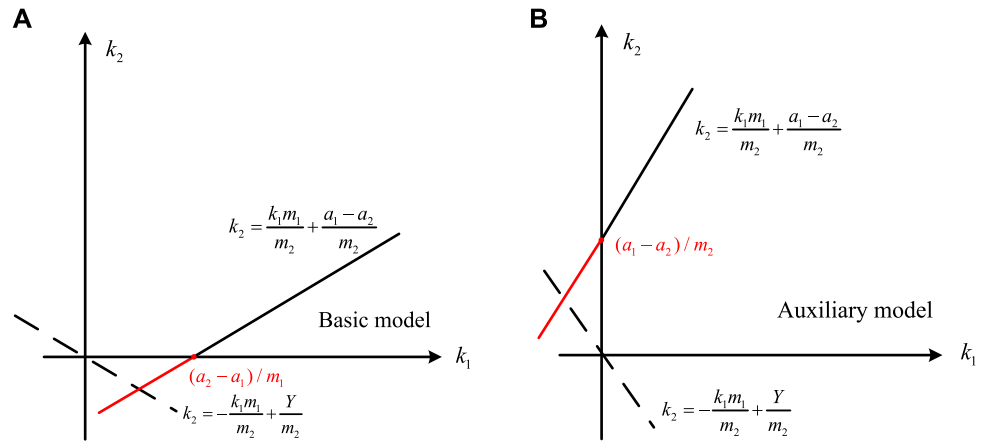

FIGURE 4 | (A) Schematic diagram of objective function and constraint conditions in case of $a_2 > a_1$. **(B)** Schematic diagram of objective function and constraint conditions in case of $a_2 < a_1$.

$$basic\ model\begin{cases} k_1^* = \dfrac{a_2 - a_1}{m_1}, \\ k_2^* = 0, \end{cases} \quad auxiliary\ model\begin{cases} k_2^* = \dfrac{a_1 - a_2}{m_2}, \\ k_1^* = 0. \end{cases} \tag{9}$$

According to the intersection of the constraint condition and the k_i axis, we branch the ambiguity number variable. For the basic and auxiliary models, k_i or k_2 component is branched, respectively, denoted as LP_1 and LP_2 models.

$$basic\ model\begin{cases} (LP_1)\begin{cases} (LP) \\ k_1 \le \left[\dfrac{a_2 - a_1}{m_1}\right] \end{cases} \\ (LP_2)\begin{cases} (LP) \\ k_1 \ge \left[\dfrac{a_2 - a_1}{m_1}\right] + 1 \end{cases} \end{cases} \quad auxiliary\ model\begin{cases} (LP_1)\begin{cases} (LP) \\ k_2 \le \left[\dfrac{a_1 - a_2}{m_2}\right] \end{cases} \\ (LP_2)\begin{cases} (LP) \\ k_2 \ge \left[\dfrac{a_1 - a_2}{m_2}\right] + 1 \end{cases} \end{cases} \tag{10}$$

where [] is the rounding function. As shown in **Figure 4**, whether it is the basic model or the auxiliary model, if only the traversal of the ambiguity number to positive direction of the coordinate axis is considered, only the LP_2 models need to be considered.

According to **Eq. 5**, the objective function expression can be changed:

$$k_2 = -\frac{k_1 m_1}{m_2} + \frac{Y}{m_2}. \tag{11}$$

The initial values of the ambiguity numbers k_1 and k_2 for the two models can be set:

$$basic\ model\begin{cases} k_1 = \left[\dfrac{a_2 - a_1}{m_1}\right] + 1, \\ k_2 = 0, \end{cases} \quad auxiliary\ model\begin{cases} k_2 = \left[\dfrac{a_1 - a_2}{m_2}\right] + 1, \\ k_1 = 0. \end{cases} \tag{12}$$

The traversal path is determined by the slope. If $m_1/m_2 > 1$, then k_1 is traversed. If $m_1/m_2 < 1$, then k_2 is traversed.

In case of $m_1/m_2 > 1$, as shown in **Figure 5**, k_1 is incremented by one unit length in turn, and then it is determined whether k_2 satisfies an integer according to **Eq. 13**, until the integer solution corresponding to the minimum objective function value under this following condition is found:

$$k_2 = \frac{k_1 m_1}{m_2} + \frac{a_1 - a_2}{m_2}. \tag{13}$$

For the basic model, because of $m_1/m_2 > 1$, the initial value has the following restrictions: k_1 is traversed sequentially from 1. For the auxiliary model, k_1 is traversed directly from 0.

$$0 < \frac{a_2 - a_1}{m_1} < \frac{a_2 - a_1}{m_2} < 1. \tag{14}$$

In case of $m_1/m_2 < 1$, as shown in **Figure 6**, k_2 is incremented by one unit length in turn, and then it is determined whether k_1 satisfies an integer according to **Eq. 15**, until the integer solution corresponding to the minimum objective function value under this following condition is found.

$$k_1 = \frac{k_2 m_2}{m_1} + \frac{a_2 - a_1}{m_1}. \tag{15}$$

For the basic model, k_2 is traversed directly from 0. For the auxiliary model, because of $m_1/m_2 < 1$, the initial value has the following restrictions: k_2 is traversed sequentially from 1.

$$0 < \frac{a_1 - a_2}{m_2} < \frac{a_1 - a_2}{m_1} < 1. \tag{16}$$

So far, the positive traversal of determining the ambiguity number k_i based on the relationship between a_1 and a_2 has ended. The negative traversal can solve the corresponding negative ambiguity number according to the aforementioned theories.

Ambiguity Number Solving in a Special Case

In case of $a_1 = a_2$, as shown in **Figure 7**, the intercept between the constraint condition and horizontal axis becomes 0, and the optimal solution can start from the point (0,0). In this situation, the ambiguity numbers have all satisfied the integer condition, so there is no need to traverse. The corresponding optimal integer solution are as follows:

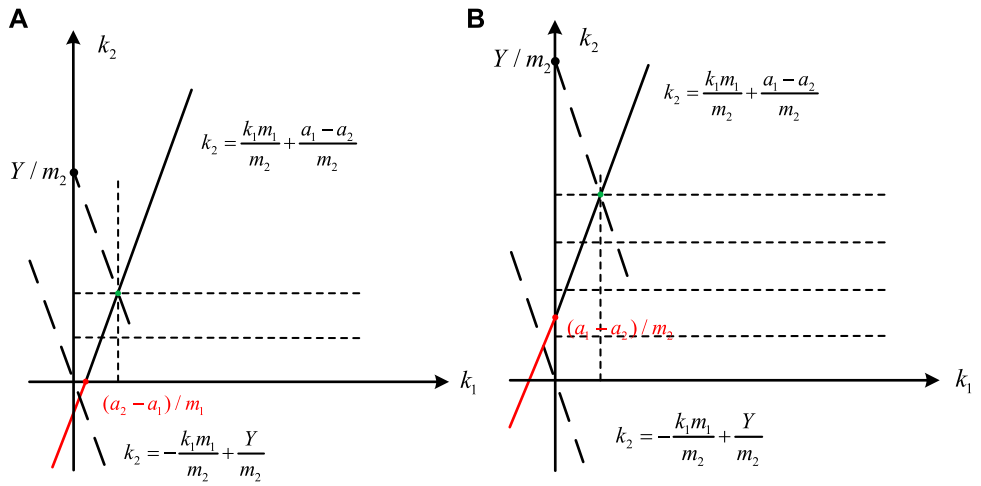

FIGURE 5 | (A) Schematic diagram of k_1 increasing sequentially when $a_2 > a_1$ and $m_1/m_2 > 1$.**(B)** Schematic diagram of k_1 increasing sequentially when $a_2 < a_1$ and $m_1/m_2 > 1$.

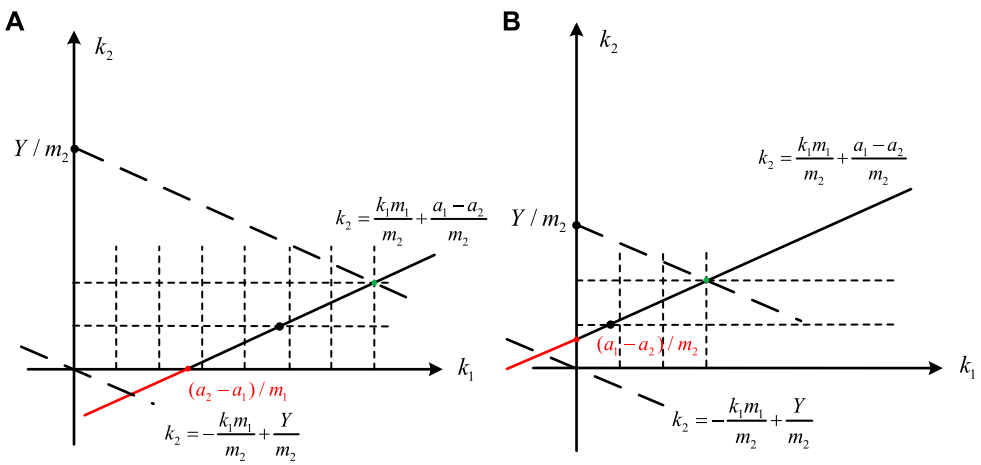

FIGURE 6 | (A) Schematic diagram of k_2 increasing sequentially when $a_2 > a_1$ and $m_1/m_2 < 1$. **(B)** Schematic diagram of k_2 increasing sequentially when $a_2 < a_1$ and $m_1/m_2 < 1$.

$$k_1 = k_2 = 0. \tag{17}$$

It can be seen from the aforementioned analysis that after transforming the dual-baseline InSAR phase unwrapping problem into the PIP problem, we only need to find the corresponding algorithm to solve the integer K, and there is no requirement for the adjacent interferometric phase difference to be less than half a period. Therefore, the proposed method can extend the non-ambiguity interval to $[-m\pi, m\pi)$ and also has a better unwrapping ability in the phase under-sampling region. In addition, the ratio of m_1 and m_2 determines the slope of the straight line, and the pure integer programming phase unwrapping method also weakens the baseline requirement of interferometric pairs. As long as the two baselines have different lengths, the unwrapping phase can be effectively solved.

Optimized Algorithm Using the Axis Symmetry Theory

In order to further improve unwrapping efficiency, the axis symmetry theory is also introduced in this proposed method. As shown in **Figure 8**, if a_1 and a_2 and m_1 and m_2 in the optimal solution parameters are interchanged, the auxiliary model can be transformed into the basic model. Just as that the black line represents the basic model, and the blue line represents the auxiliary model; the two models are symmetric about the line $k_1 = k_2$. Therefore, in this case, the corresponding ambiguity number can be solved by repeating the aforementioned steps. The axis symmetry theory can optimize the four traversing approaches to be considered into two traversing approaches (**Figure 9**), which reduces the storage space of traversing variables and improves operating efficiency.

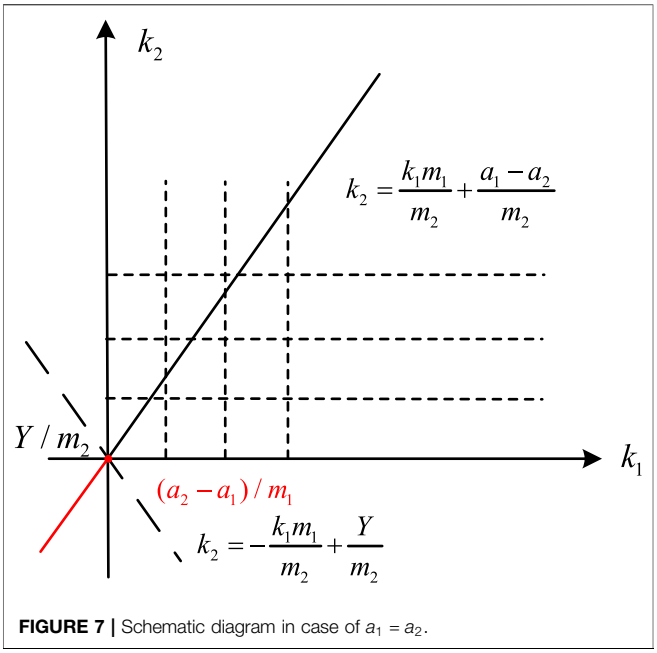

FIGURE 7 | Schematic diagram in case of $a_1 = a_2$.

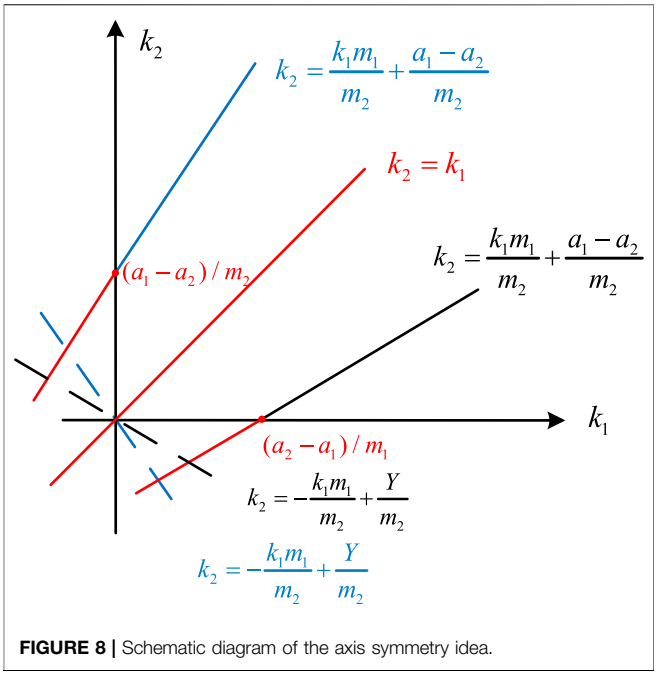

FIGURE 8 | Schematic diagram of the axis symmetry idea.

RESULTS AND DISCUSSION

Results and Discussion of Simulation Data

In order to verify the feasibility of the branch and bound PIP–PU algorithm for dual-baseline InSAR, the first experiment is performed on the simulated data using the sinc function. **Figures 10A,B** show the three-dimensional (3D) and two-dimensional (2D) digital elevation model (DEM), respectively. **Figures 10C,D**, respectively, show the interferograms of the short and long baselines.

After unwrapping by the branch and bound PIP–PU method, the 3D map of the solved ambiguity numbers, unwrapping results, and phase errors are shown in **Figure 11**. The solved ambiguity numbers are similar to the integer layer of 3D DEM. The longer the baseline, the denser the solved ambiguity numbers, and the closer the 3D map is to the 3D DEM. This is because the baseline length is proportional to the absolute phase, and the larger the absolute phase, the larger the solved ambiguity numbers. The unwrapping results show that the overall phases have good continuity; the phase errors are not only concentrated around 0, but also the order of magnitude can reach 10–15, which prove that this proposed algorithm based on PIP mathematical ideas can effectively guarantee the accuracy of unwrapping.

Results and Discussion of Noisy Dual-Baseline Interferogram

In the second experiment, we select Isolation Peak National Park data to verify the effectiveness and noise robustness performance of this proposed method. **Figures 12A,B** show 2D and 3D DEM. **Figures 12C,D** show simulated noisy interferograms with 105 m baseline and 189 m baseline, respectively, in which we added a random phase noise with a mean value of 0 and a variance of 0.1 rad^2. The main parameters are shown in **Table 1**.

There exists phase under-sampling area in the red frame of the aforementioned interferograms. The unwrapping results of 105 m and 189 m baseline interferograms using the branch and bound PIP–PU method are shown in **Figures 13A,C**, respectively, which are in good agreement with **Figure 12A**. By further making the difference between the unwrapping result and the original reference phase, the phase error distribution map is as shown in **Figures 13B,D**. Better unwrapping results can be obtained even in phase under-sampling areas and abrupt topographic change areas. Compared with **Figures 11C,F**, although the phase error is distributed around 0, the order of magnitude becomes significantly large. It shows that this proposed algorithm is relatively sensitive to the noise. The next step should be to improve the noise robustness ability of this algorithm. But even so, the unwrapping accuracy of the proposed algorithm is still optimal, which will be proved in the following quantitative analysis.

To further verify the effectiveness of the proposed method, the branch-cut method, quality-guided method, LS method, and MCF method are used to unwrap the 105 m baseline interferogram. **Figures 13E,F** show the unwrapping results of the branch-cut method. There exist obvious phase errors in the phase under-sampling area of the red frame, and the unwrapping effect is also poor in the abrupt topographic change area. **Figures 13G,H** show the unwrapping results of the quality-guided method. There is no excessive deviation, but the unwrapping effect is also poor in the phase under-sampling area and the abrupt topographic change area. **Figures 13I,J** show the results of the LS method. From the overall point of view, the phase continuity is guaranteed. However, the unwrapping result has

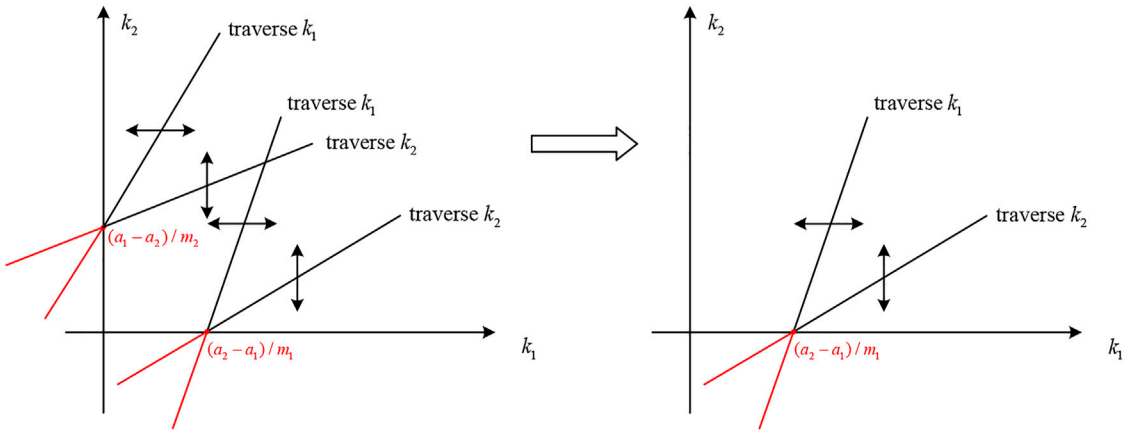

FIGURE 9 | Simplified schematic diagram of the ambiguity number traversal path.

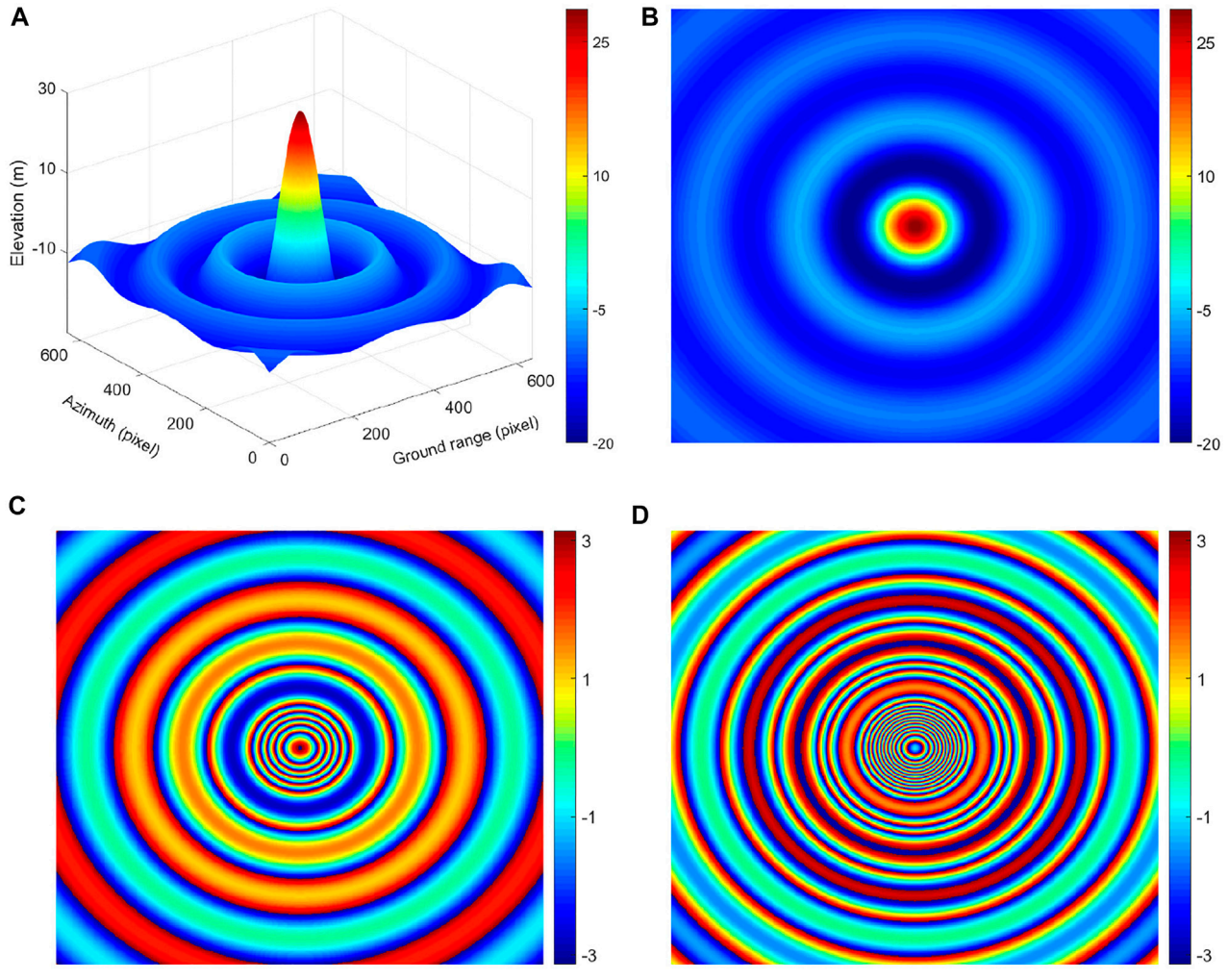

FIGURE 10 | Sinc function. **(A)** 3D DEM (m). **(B)** 2D DEM (m). **(C)** Simulated short-baseline interferogram (rad). **(D)**Simulated long-baseline interferogram (rad).

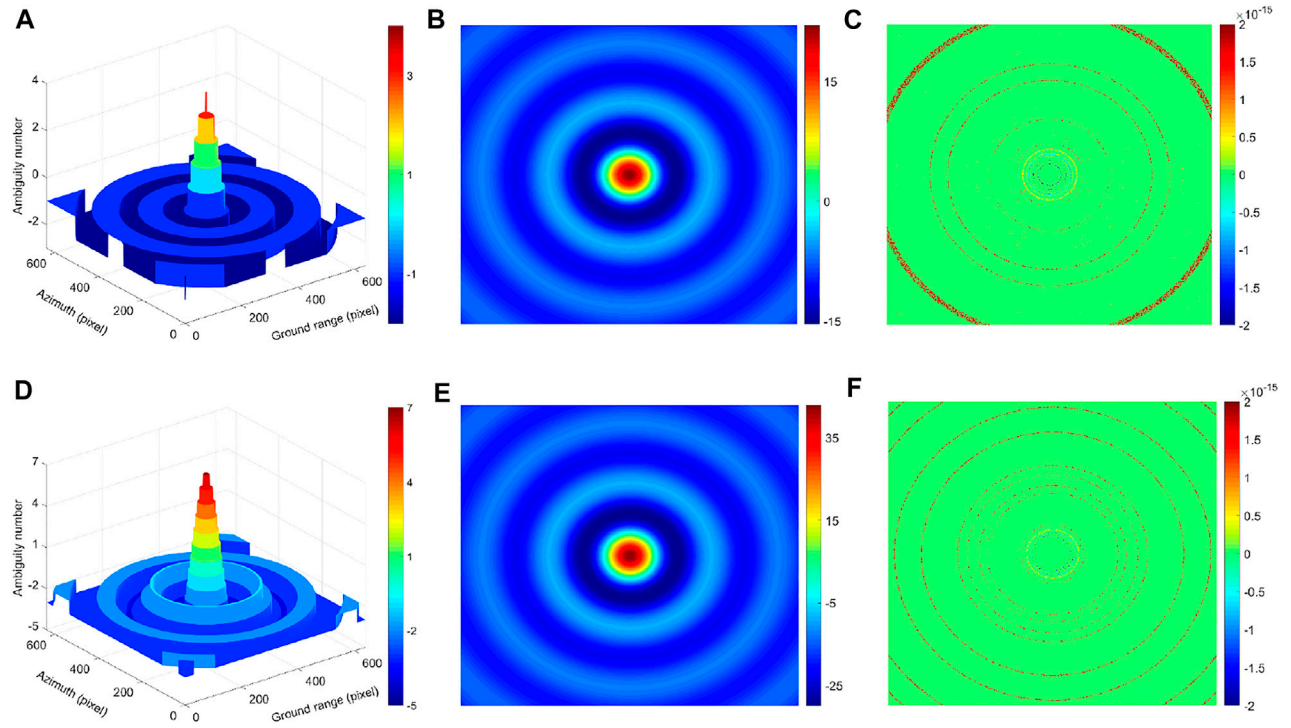

FIGURE 11 | (A) 3D map of the solved ambiguity numbers for short-baseline interferogram. **(B)** Unwrapping results for short-baseline interferogram (rad). **(C)** Phase error distribution map for short-baseline interferogram (rad). **(D)** 3D map of the solved ambiguity numbers for long-baseline interferogram. **(E)** Unwrapping results for long-baseline interferogram (rad). **(F)** Phase error distribution map for long-baseline interferogram (rad).

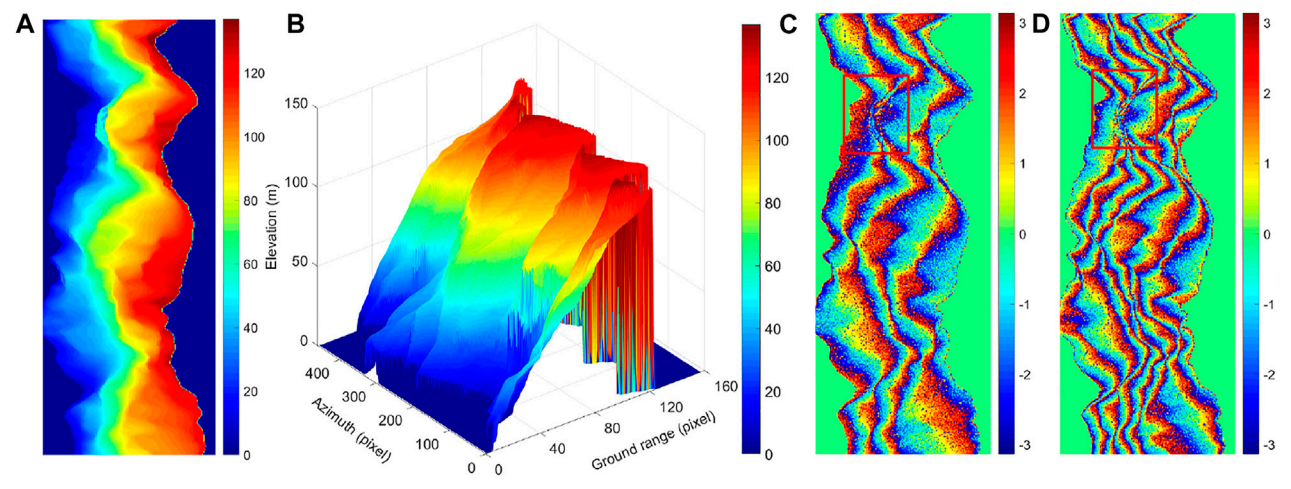

FIGURE 12 | Isolation Peak National Park, United States **(A)** 2D DEM (m). **(B)** 3D DEM (m). **(C)** Simulated interferogram with 105 m baseline (rad). **(D)** Simulated interferogram with 189 m baseline (rad).

TABLE 1 | Main parameters of the interferograms.

Orbit altitude/km	Image size/pixel×pixel	Incidence angle/(°)	Wavelength/m	Baseline 1/m	Baseline 2/m
600	458 × 157	30	0.057	105	189

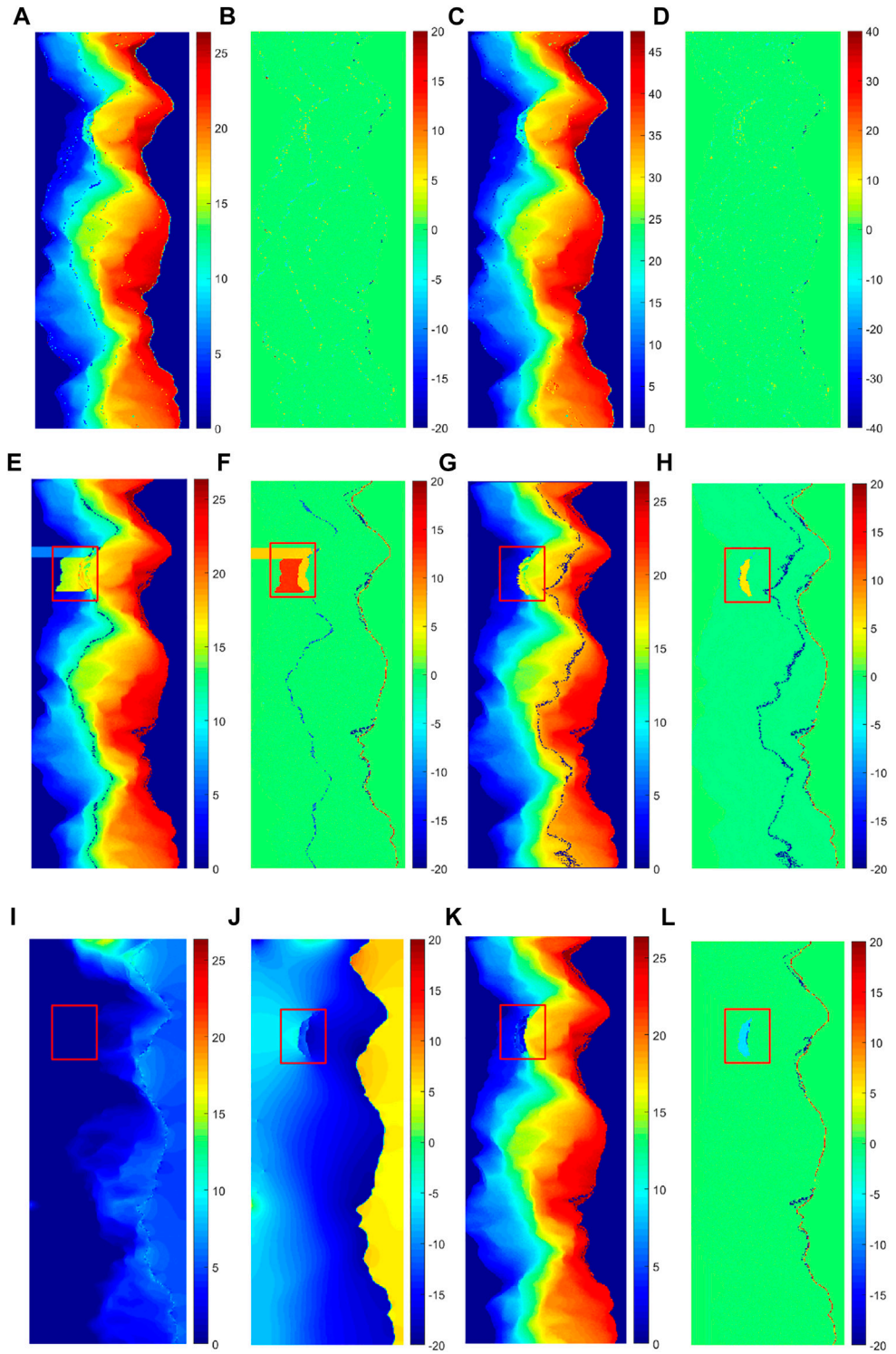

FIGURE 13 | (A) Unwrapping results of the PIP method based on 105 m baseline (rad). **(B)** Phase error distribution map of the PIP method based on 105 m baseline (rad). **(C)** Unwrapping results of the PIP method based on 189 m baseline (rad). **(D)**Phase error distribution map of the PIP method based on 189 m baseline (rad). **(E)** Unwrapping results of the branch-cut method based on 105 m baseline (rad). **(F)** Phase error distribution map of branch-cut method based on 105 m baseline (rad). **(G)** Unwrapping results of the quality-guided method based on 105 m baseline (rad). **(H)** Phase error distribution map of the quality-guided method based on 105 m baseline (rad). **(I)** Unwrapping results of the LS method based on 105 m baseline (rad). **(J)** Phase error distribution map of the LS method based on 105 m baseline (rad). **(K)** Unwrapping results of the MCF method based on 105 m baseline (rad). **(L)** Phase error distribution map of the MCF method based on 105 m baseline (rad).

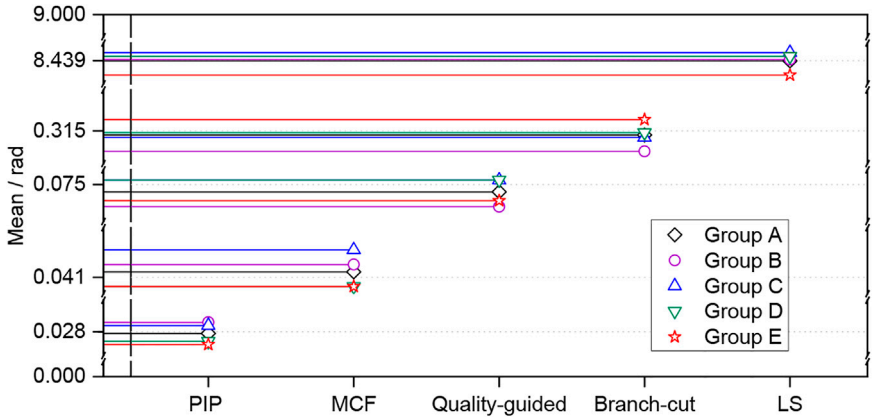

FIGURE 14 | Mean scatter plot for phase errors of five groups of repeated experiments.

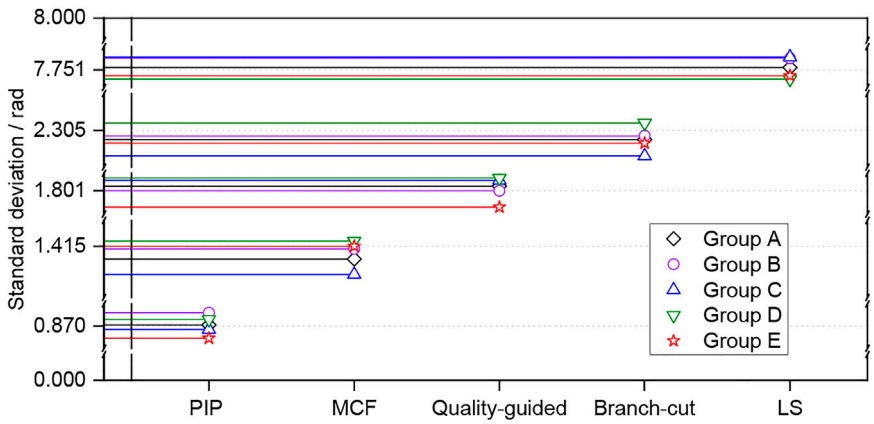

FIGURE 15 | Standard deviation scatter plot for phase errors of five groups of repeated experiments.

too much phase deviation. Most of the data are almost 10 rad different from the original phase, and some even reach 20 rad. The main reason is that the discrete phase gradient estimation cannot reflect the true phase gradient, which introduces the large error. **Figures 13K,L** show the results of the MCF method. The number of error points is greatly reduced, especially in the left area. The PU effect has been greatly improved but is still not ideal in phase under-sampling areas and abrupt topographic change areas.

Taking into account the randomness of the noise generated by the simulation experiment, five groups of repeated experiments were performed by adding the same level of noise to the interferograms. **Figures 14**, **15** show the scatter plots of the mean and standard deviation of phase errors. Different algorithms focus around a different number. Both the error indicators of this proposed algorithm are always the smallest, followed by the MCF method, quality-guided method, branch-cut method, and LS method. **Table 2** gives the average values of the five groups of repeated experiments. The branch-cut method has a large phase error mean and standard deviation, so the unwrapping effect is poor, but the unwrapping efficiency is higher. Compared with it, the quality-guided method has a lower mean and standard deviation, but the unwrapping efficiency is the worst. The LS method has the highest unwrapping efficiency, but the mean and standard deviation are the largest, and the unwrapping effect is also the worst. The error indicators of the MCF method are obviously smaller, and the unwrapping effect is better, but the diversity of network planning results in its low efficiency. For the PIP–PU method, the mean and standard deviation of phase errors are greatly reduced, and the unwrapping efficiency is sub-optimal. The reason is that the PIP–PU method uses rigorous mathematical expressions to accurately solve the ambiguity number, which is equivalent to realize the point-by-point unwrapping of the four neighborhoods of each reference point. Even in the phase abrupt change area, the ambiguity number can also be accurately solved, so the unwrapping accuracy is the highest. In addition, the traversal method adopts four-neighborhood expansion, which is similar to the branch-cut traversal method, so the time cost is not much

TABLE 2 | Evaluation of different phase unwrapping methods.

Phase unwrapping method	Mean/rad	Standard deviation/rad	Unwrapping efficiency/s
Branch-cut method	0.3145	2.3045	3.46
Quality-guided method	0.0745	1.8014	43.52
LS method	8.4385	7.7512	1.42
MCF method	0.0413	1.4145	6.37
PIP method	0.0278	0.8701	3.04

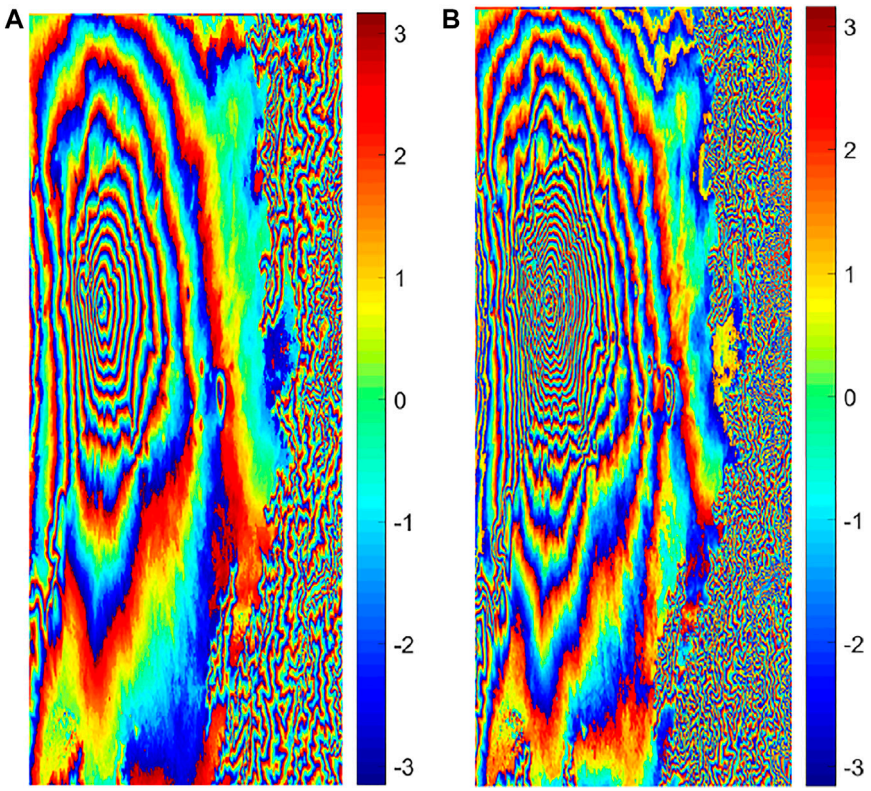

FIGURE 16 | Real Etna ERS-1/2 interferograms. **(A)** Short-baseline interferogram (rad). **(B)** Long-baseline interferogram (rad).

different from the branch-cut method. Therefore, according to the overall performance evaluation, the unwrapping effect is relatively better, which verifies the effectiveness of the proposed method.

Results and Discussion of Real Dual-Baseline Interferogram

In the third experiment, we take the real Etna ERS-1/2 interferogram data (5,186 × 1998 pixels) to evaluate the practicality of this proposed method, which are shown in **Figure 16**.

Figures 17A,C show the 3D maps of the solved ambiguity numbers corresponding to different baseline interferograms. It can be seen that the terrain has an extreme value of the ambiguity number in the left area, so there may exist a towering terrain. Compared with the unwrapping results in **Figures 17B,D**, the phase distribution regularity is also consistent with that of the solved ambiguity number. **Figure 17E** shows the re-wrapped result of the long-baseline unwrapping phase, which is highly consistent with the original interferogram (**Figure 16B**), then the difference between the two can get the phase error distribution map as shown in **Figure 17F**, and the errors are almost 0. Finally, the inverted DEM using the long-baseline unwrapping result is shown in **Figure 17G**. Compared with the 3D maps of the solved ambiguity numbers (**Figures 17A,C**), the distribution regularity of the three are also highly consistent, which is sufficient to prove the effectiveness and practicality of the proposed algorithm.

The representative algorithms were selected from the path-following type, the minimum norm type, and the optimal estimation type for this long-baseline unwrapping experiment. The unwrapping results of the branch-cut method, LS method, and MCF method are shown in **Figures 18A–C**, respectively. Since the integral path fails to bypass the residual point, the error

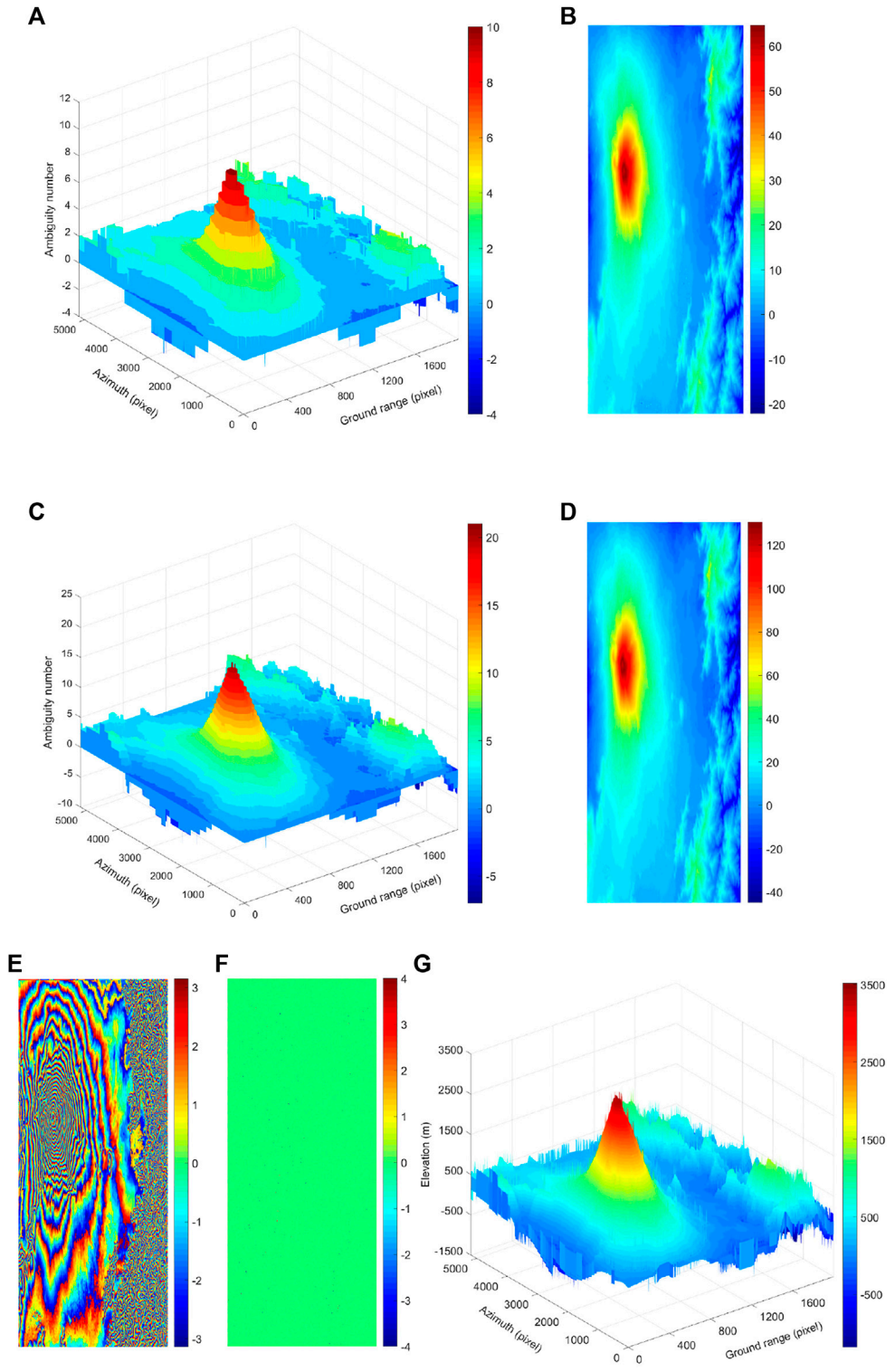

FIGURE 17 | Unwrapping results of real data. **(A)** 3D map of the solved ambiguity numbers for short-baseline interferogram. **(B)** Unwrapping results for short-baseline interferogram (rad). **(C)** 3D map of the solved ambiguity numbers for long-baseline interferogram. **(D)** Unwrapping results for long-baseline interferogram (rad). **(E)** Re-wrapped results of long-baseline (rad). **(F)** Phase errors between re-wrapped results and original interferogram (rad). **(G)** Inverted DEM (m).

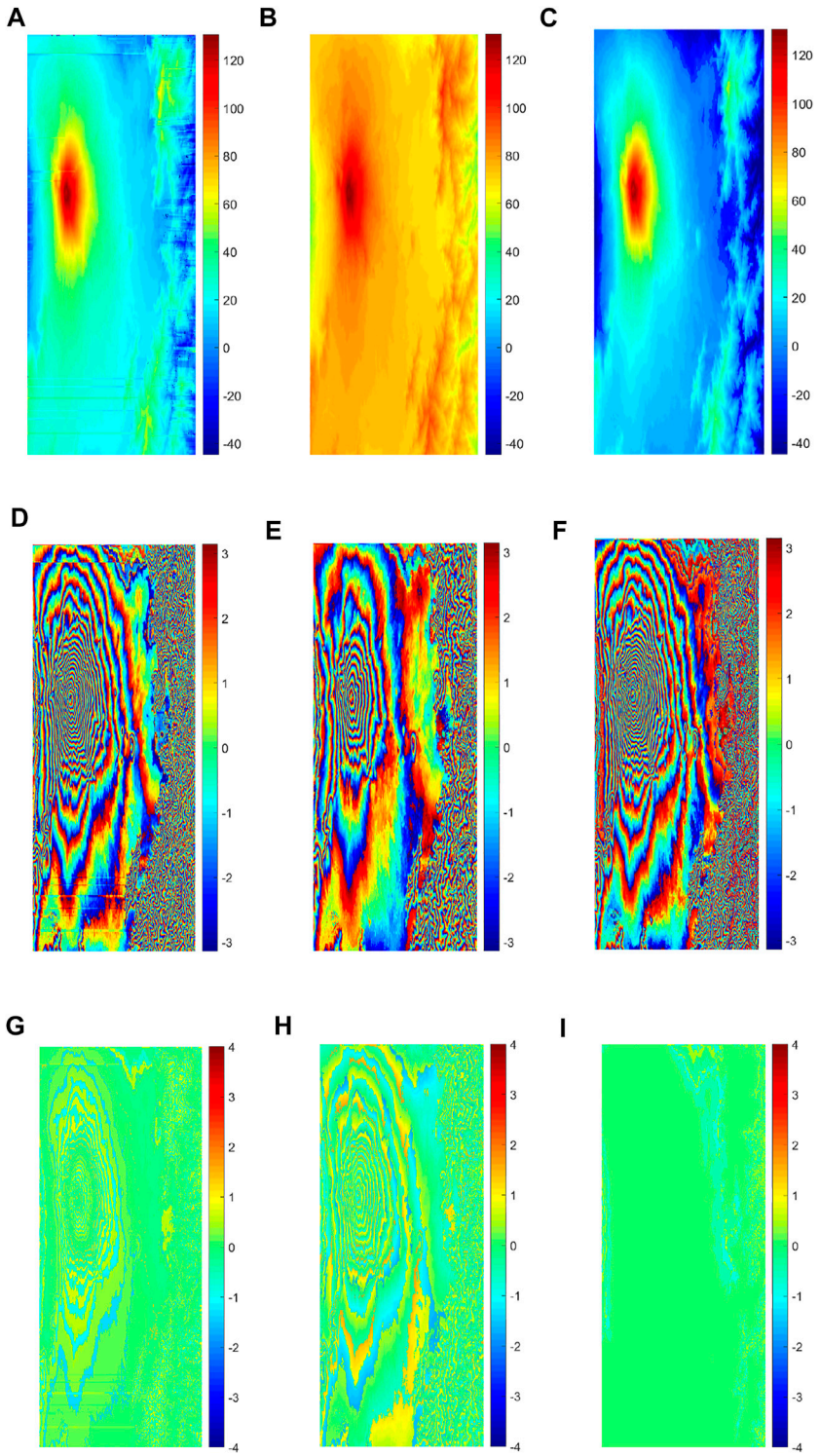

FIGURE 18 | Unwrapping results of real data. **(A)** Branch-cut method (rad). **(B)** LS method (rad). **(C)** MFC method (rad). **(D)** Re-wrapped results of the branch-cut method (rad). **(E)** Re-wrapped results of the LS method (rad). **(F)** Re-wrapped results of the MFC method (rad). **(G)** Phase errors between re-wrapped results and original interferogram of the branch-cut method (rad). **(H)** Phase errors between re-wrapped results and original interferogram of the LS method (rad). **(I)** Phase errors between re-wrapped results and original interferogram of the MFC method (rad).

propagation leads to a large number of wrong unwrapped points in the whole row of unwrapped results of the branch-cut method. The results of the LS method are similar to the unwrapping effect of the Isolation Peak National Park in the second experiment. Although the phase continuity is guaranteed, the phase errors are relatively large. The results of the MCF method are particularly good visually.

Figures 18D–F show the re-wrapped results of long-baseline unwrapping phase, and **Figures 18G–I** show the phase error between re-wrapped results and original interferogram. Comparing **Figures 17E,F**, the re-wrapped results of the branch-cut method still show a large number of wrong unwrapped points in the whole row, and phase errors from the original interferogram exhibit a ring-shaped distribution. The re-wrapped results of the LS method appear as sparser fringes, missing details of the original interferogram, so phase errors are so large that they also exhibit a more obvious ring-shaped distribution. The re-wrapped results and phase error of the MCF method are highly consistent with the original interferogram (**Figure 16B**), and there are some differences only in the right area. Therefore, from the visual effect of unwrapping results for real data, the proposed algorithm in this article also has the highest accuracy.

CONCLUSION

According to the similarity between PIP problem and solving the number of integral cycles in PU, the former is applied to the PU for dual-baseline InSAR. Taking the intercept on the vertical axis as the objective function and a ray as the constraint condition, the PIP–PU model is constructed, and a new branch and bound PIP–PU algorithm is deduced and described in detail by graphical means. This algorithm not only expands the non-ambiguity interval but also weakens the requirement of the baseline. As long as the two baselines have different lengths, the PU can be effectively solved. Finally, the two sets of simulated data by the sinc function and Isolation Peak National Park DEM and one set of real data from Etna volcano are used to conduct PU experiments. Compared with the branch-cut method, quality-guided method, LS method, and MCF method, this proposed method has more advantages in phase under-sampling areas and abrupt topographic change areas. Both visual effects and quantitative results prove the feasibility, effectiveness, and practicability of the PIP–PU algorithm. In the follow-up research, it is necessary to further verify the noise robustness ability of the PIP–PU algorithm.

DATA AVAILABILITY STATEMENT

The original contributions presented in the study are included in the article/Supplementary Materials, Further inquiries can be directed to the corresponding authors.

AUTHOR CONTRIBUTIONS

HL designed the research, proposed the method, and developed the main idea. JY contributed to experiment and analysis. QH supervised the work. GL contributed to modifying the structure of the manuscript and proofreading the manuscript. ML contributed to correcting the language and helped in layout of the manuscript. All authors have read and agreed to the published version of the final manuscript.

FUNDING

This work was supported by the National Natural Science Foundation of China (No. 41901411), Henan Provincial Science and Technology Research Project (No. 212102310052), Henan Youth Talent Support Program (No. 2020HYTP010), Training Plan for Young Backbone Teachers of Colleges and Universities in Henan Province (No. 2021GGJS073), Key Scientific Research Project of Colleges and Universities in Henan province (No. 19A420008), and Joint Fund of Collaborative Innovation Center of Geo-Information Technology for Smart Central Plains, Henan Province and Key Laboratory of Spatiotemporal Perception and Intelligent Processing, Ministry of Natural Resources (No. 211103).

ACKNOWLEDGMENTS

The authors would like to gratefully acknowledge GuoWang Jin for his SAR technical support. The authors also thank the anonymous reviewers for their constructive comments and suggestions.

REFERENCES

Bouras, I., Figueiredo, R., Poss, M., and Zhou, F. (2020). Minimizing Energy and Link Utilization in ISP Backbone Networks with Multi-Path Routing: A Bi-level Approach. *Optim. Lett.* 14, 209–227. doi:10.1007/s11590-019-01505-x

Chen, Q., Yang, Y. H., Liu, G. X., Cheng, H. Q., and Liu, W. T. (2012). InSAR Phase Unwrapping Using Least Squares Method with Integer Ambiguity Resolution and Edge Detection. *Acta Geod. Cartogr. Sinica* 41, 441–448.

Costalltilli, M. (1998). A Novel Phase Unwrapping Method Based on Network Programming. *IEEE Transaction Geoscience Remote Sens.* 36, 813–821. doi:10.1109/36.673674

Department of Mathematics of Tongji University (2003). *Engineering Mathematics, Linear Algebra*. 6th Edition. Beijing: Higher Education Press.

Dong, Y., Jiang, H., Zhang, L., and Liao, M. (2018). An Efficient Maximum Likelihood Estimation Approach of Multi-Baseline SAR Interferometry for Refined Topographic Mapping in Mountainous Areas. *Remote Sens.* 10, 454–474. doi:10.3390/rs10030454

Flynn, T. J. (1997). Two-dimensional Phase Unwrapping with Minimum Weighted Discontinuity. *J. Opt. Soc. Am. A* 14, 2692–2701. doi:10.1364/josaa.14.002692

Gao, Y., Zhang, S., Li, T., Chen, Q., Zhang, X., and Li, S. (2019). Refined Two-Stage Programming Approach of Phase Unwrapping for Multi-Baseline SAR Interferograms Using the Unscented Kalman Filter. *Remote Sens.* 11, 199–217. doi:10.3390/rs11020199

Ge, S. Q., Chen, L., Ding, Z. G., and Long, T. (2013). A Robust Multifrequency Phase Unwrapping Method Based on Gradient Reconstruction. *Acta Geod. Cartogr. Sinica* 42, 367–373+396.

Goldstein, R. M., Zebker, H. A., and Werner, C. L. (1988). Satellite Radar Interferometry: Two-Dimensional Phase Unwrapping. *Radio Sci.* 23, 713–720. doi:10.1029/rs023i004p00713

Jiang, Z. B., Wang, J., Song, Q., and Zhou, Z. M. (2019). A Searched-form Robust Chinese Remainder Theorem Based Multi-Baseline Phase Unwrapping Algorithm. *J. Natl. Univ. Def. Technol.* 41, 72–79. doi:10.11887/j.cn.201901011

Jiang, Z., Wang, J., Song, Q., and Zhou, Z. (2017). A Refined Cluster-Analysis-Based Multibaseline Phase-Unwrapping Algorithm. *IEEE Geosci. Remote Sens. Lett.* 14 (9), 1565–1569. doi:10.1109/lgrs.2017.2723050

Jin, B., Guo, J., Wei, P., Su, B., and He, D. (2018). Multi-baseline InSAR Phase Unwrapping Method Based on Mixed-integer Optimisation Model. *IET Radar, Sonar & Navig.* 12, 694–701. doi:10.1049/iet-rsn.2017.054310.1049/iet-rsn.2017.0543

Jin, G. W., Xu, Q., and Zhang, H. M. (2014). *Synthetic Aperture Radar Interferometry*. Beijing, China: National Defense Industry Press.

Jin, G. W., Zhang, H. M., Xu, Q., Qin, Z. Y., and Shi, Q. J. (2012). Phase Unwrapping Algorithm with Difference Filter for Multi-Band InSAR. *Acta Geod. Cartogr. Sinica* 41, 434–440+448. doi:10.3788/gzxb20124109.1130

Levitin, E., and Tichatschke, R. (1998). A Branch-And-Bound Approach for Solving a Class of Generalized Semi-infinite Programming Problems. *J. Glob. Optim.* 13, 299–315. doi:10.1023/A:1008245113420

Liao, M. S., and Lin, H. (2003). *Synthetic Aperture Radar Interferometry-Principle and Signal Processing*. Beijing, China: The Publishing House of Surveying and Mapping, 1–14.

Liu, G. L., Hao, H. D., Yan, M., and Tao, Q. X. (2011). Phase Unwrapping Algorithm by Using Kalman Filter Based on Topographic Factors. *Acta Geod. Cartogr. Sinica* 40, 283–288. doi:10.1109/OCEANSSYD.2010.5603794

Liu H, H., Xing, M., and Bao, Z. (2015). A Novel Mixed-Norm Multibaseline Phase-Unwrapping Algorithm Based on Linear Programming. *IEEE Geosci. Remote Sens. Lett.* 12, 1086–1090. doi:10.1109/lgrs.2014.2381666

Liu H T, H. T., Mengdao Xing, M. D., and Zheng Bao, Z. (2015). A Cluster-Analysis-Based Noise-Robust Phase-Unwrapping Algorithm for Multibaseline Interferograms. *IEEE Trans. Geosci. Remote Sens.* 53 (1), 494–504. doi:10.1109/tgrs.2014.2324595

Liu, H., Bai, Z. C., Li, G. S., Tian, D. Y., and Wang, B. C. (2019). *Radar Interferometry-DEM Aided Interference and Deformation Monitoring Technology*. Beijing, China: Geological Publishing House, 54–70.

Liu, H., Jin, G. W., Zhang, H. M., and Xu, Q. (2017). Phase Unwrapping Assisted by DEM of InSAR for Mountainous Terrain. *J. Geomatics Sci. Technol.* 34, 215–220. doi:10.3969/j.issn.1673-6338.2017.02.019

Liu, H. T. (2015). *Study on Multi-Baseline Phase Unwrapping Algorithm*. Xi'an: Xidian University, 19–29.

Liu, H., and Xu, Q. (2018). Interference Processing for Zero Intermediate Frequency Multi-Baseline InSAR Assisted by DEM. *J. Henan Normal Univ. Nat. Sci. Ed.* 46, 42–47. doi:10.16366/j.cnki.1000-2367.2018.05.007

Long, J. P., Ding, X. L., Li, Z. W., Xiang, R., and Feng, G. C. (2008). LAMBDA Method Applied to Phase Unwrapping in CR-InSAR. *J. Geodesy Geodyn.* 3, 100–103. doi:10.14075/j.jgg.2008.03.007

Ma, L. T., Lu, X. P., and Zhou, Y. S. (2020). An Improved Multi-Baseline InSAR Unwrapping Algorithm Based on Maximum Likelihood Estimation[J]. *Sci. Surv. Mapp.* 45, 123–129. doi:10.16251/j.cnki.1009-2307.2020.08.019

Markus, E. (2016). Accelerating Phase Unwrapping Based on Integer Linear Programming by Processing of Subgraphs. *IEEE Transaction Geosicience Remote Sens.*, 6441–6444. doi:10.1109/IGARS.2016.7730683

Omer, O., Murat, E., and Ilker, B. (2020). Reliable Communication Network Design: The Hybridisation of Metaheuristics with the Branch and Bound Method. *J. Operational Res. Soc.* 71, 784–799. doi:10.1080/01605682.2019.1582587

Si, Q., Wang, Y., Deng, Y. K., Li, N., and Zhang, H. (2017). A Novel Cluster-Analysis Algorithm Based on MAP Framework for Multi-Baseline InSAR Height Reconstruction. *J. Radars* 6, 640–652. doi:10.12000/JR17043

Takajo, H., and Takahashi, T. (1988). Noniterative Method for Obtaining the Exact Solution for the Normal Equation in Least-Squares Phase Estimation from the Phase Difference. *J. Opt. Soc. Am. A* 5, 1818–1827. doi:10.1364/josaa.5.001818

Tang, X. M., Li, T., Gao, X. M., Chen, Q. F., and Zhang, X. (2018). Research on Key Technologies of Precise InSAR Surveying and Mapping Application Using Automatic SAR Imaging. *Acta Geod. Cartogr. Sinica* 47, 730–740. doi:10.11947/j.AGCS.2018.20170621

Wang, C., Zhang, H., and Liu, Z. (2002). *Spaceborne Synthetic Aperture Radar Interferometry*. Beijing, China: Science Press, 2–24.

Wei, X., Chang, E. C., Kwoh, L. K., Lim, H. H., and Wang, C. A. (1994). Phase-unwrapping of SAR Interferogram with Multi-Frequency or Multi-Baseline. *IEEE Int. Geoscience Remote Sens. Symposium* 2, 730–732. doi:10.1109/IGARSS.1994.399243

Xie, X. M., Sun, Y. Z., Liang, X. X., Zeng, Q. N., and Zheng, Z. H. (2020). Recursive Estimation Method of Cubature Kalman Filtering Local Polynomial Coefficients for Phase Unwrapping. *Acta Geod. Cartogr. Sinica* 49, 1023–1031. doi:10.11947/j.AGCS.2020.20190385

Yu, H., Lan, Y., Yuan, Z., Xu, J., and Lee, H. (2019). Phase Unwrapping in InSAR : A Review. *IEEE Geosci. Remote Sens. Mag.* 7, 40–58. doi:10.1109/mgrs.2018.2873644

Yu, H., Li, Z., and Bao, Z. (2011). A Cluster-Analysis-Based Efficient Multibaseline Phase-Unwrapping Algorithm. *IEEE Trans. Geosci. Remote Sens.* 49 (1), 478–487. doi:10.1109/tgrs.2010.2055569

Yu, H. W., and Bao, Z. (2013). L1-norm Method for Multi-Baseline InSAR Phase Unwrapping. *J. Xidian Univ.* 40 (04), 37–41. doi:10.3969/j.issn.1001-2400.2013.04.006

Yu, H. W., Cao, N., Lan, Y., and Xing, M. D. (2020). Multisystem Interferometric Data Fusion Framework: A Three-step Sensing Approach. *IEEE Trans. Geoscience Remote Sens.* 59, 8501–8509. doi:10.1109/TGRS.2020.3045093

Yu, H. W., and Hu, X. (2021). Knowledge-Aided InSAR Phase Unwrapping Approach. *IEEE Trans. Geoscience Remote Sens.* 5, 1–8. doi:10.1109/TGRS.2021.3081039

Yu, H. W., and Lan, Y. (2016). Robust Two-Dimensional Phase Unwrapping for Multibaseline SAR Interferograms: A Two-Stage Programming Approach. *IEEE Trans. Geoscience Remote Sens.* 54, 5217–5225. doi:10.1109/TGRS.2016.2558541

Zhang, H. M., Jin, G. W., Xu, Q., and Qin, Z. Y. (2011a). Phase Unwrapping Algorithm with Difference Filtering for Multi-Baseline InSAR. *Geomatics Inf. Sci. Wuhan Univ.* 36, 1030–1034. doi:10.1007/s12583-011-0162-0

Zhang, H. M., Jin, G. W., Xu, Q., Qin, Z. Y., and Sun, W. (2011b). Application of Chinese Remainder Theorem in Phase Unwrapping for Dual-Baseline InSAR. *Acta Geod. Cartogr. Sinica* 40, 770–777. doi:10.1631/jzus.B1000265

Zhong, H.-p., Tang, J.-s., and Zhang, S. (2011). A Combined Phase Unwrapping Algorithm Based on Quality-Guided and Minimum Discontinuity for InSAR. *J. Electron. Inf. Technol.* 33, 369–374. doi:10.3724/sp.j.1146.2010.00440

Zhou, L. F., Yu, H. W., Lan, Y., and Xing, M. D. (2021). Artificial Intelligence in Interferometric Synthetic Aperture Radar Phase Unwrapping: A Review. *IEEE Geoscience Remote Sens. Mag.* 99, 2–20. doi:10.1109/mgrs.2021.3065811

Conflict of Interest: The authors declare that the research was conducted in the absence of any commercial or financial relationships that could be construed as a potential conflict of interest.

Publisher's Note: All claims expressed in this article are solely those of the authors and do not necessarily represent those of their affiliated organizations, or those of the publisher, the editors, and the reviewers. Any product that may be evaluated in this article, or claim that may be made by its manufacturer, is not guaranteed or endorsed by the publisher.